Broadband emissivity calibration of highly reflective samples at cryogenic temperatures



2012 Metrologia 49 737

(http://iopscience.iop.org/0026-1394/49/6/737)

Metrologia **49** (2012) 737–744 doi:10.1088/0026-1394/49/6/737

# Broadband emissivity calibration of highly reflective samples at cryogenic temperatures

**S I Woods[1], T M Jung[2], G T Ly[2] and J Yu[3]**

[1] National Institute of Standards and Technology, 100 Bureau Drive, Gaithersburg, MD 20899, USA
[2] Jung Research and Development Corp., 1706 U St NW #204, Washington, DC 20009, USA
[3] ITER Organization, Route de Vinon-sur-Verdon, 13115 St Paul-lez-Durance, France

E-mail: solomon.woods@nist.gov

Received 29 June 2012, in final form 10 September 2012
Published 15 October 2012
Online at stacks.iop.org/Met/49/737

**Abstract**
We have developed a technique for measuring the broadband optical emissivity of high reflectivity samples at cryogenic temperatures. This measurement method employs a primary standard optical detector with high absorptance from visible wavelengths to beyond 200 µm. Background subtraction and quantification allow determination of the emissivity with total absolute uncertainty ($k = 1$) between approximately 0.0002 and 0.002 (for emissivities between 0.0035 and 0.092) over the temperature range from 80 K to 300 K. Using the irradiance data at the detector, precise measurements of the experimental geometry and diffraction calculations, the optical power emitted by the sample can be determined. Contact thermometry measurements for the sample can then be used to find its emissivity. The emissivity calibration technique is demonstrated for large plate samples made from polished stainless steel and is also extended to calculate the separate emissivities of multiple distinct regions on a more complex sample assembly.

(Some figures may appear in colour only in the online journal)

## 1. Introduction

Accurately determining the low-temperature emissivity of highly reflective samples presents a significant challenge. Clearly, a low-emissivity sample at cryogenic temperatures will provide very little optical power to measure. In addition, background radiation from higher emissivity radiators, even when at temperatures lower than that of the measurement sample, can introduce significant uncertainty in the measurement. As a further complication, much of the thermal radiation from cryogenic sources is emitted at wavelengths of 20 µm and beyond. A successful low-uncertainty optical technique could couple a sensitive absolute detector that provides high responsivity into the far infrared with a method for careful quantification and subtraction of any background signal which can reach the detector directly or after reflection from the sample. We have developed such a technique for determining the emissivity of large area, highly reflective samples at temperatures from 80 K to 300 K, achieving to date total absolute uncertainties ($k = 1$) between approximately 0.0002 and 0.002 (for emissivities between approximately 0.0035 and 0.092).

Knowledge about the low-temperature emissivity of thermal shields or radiation baffles is important for the design of large scale cryoplants and for the thermal modelling of satellite detector systems. For instance, low-emissivity thermal shields cooled to 80 K are critical to the design of cryoplant systems for fusion reactors such as the International Thermonuclear Experimental Reactor (ITER) and Tore Supra. These thermal shields protect the superconducting magnet system from warmer components of the reactors and accurate data for their emissivities at operational temperatures are necessary for modelling of the cooling systems [1, 2]. Low-temperature emittance data on coatings and components for space satellite missions are also essential for thermal design of these systems, especially when satellite-based detectors are dedicated to infrared measurements [3–5]. A number of methods have been used to measure total broadband

  

emissivities at cryogenic temperatures, including steady-state calorimetry [4–6], dynamic calorimetric methods [7] and optical measurement of a chopped emittance signal using a bolometer [3]. The emissivity measurement technique we have developed is a background-subtracted optical method, where the detector is remote from the sample. For such a measurement, heat leakage between the source and the remote detector stage can be more easily controlled than for typical calorimetric techniques. Our use of a primary standard absolute cryogenic radiometer (ACR) for the detector enables a direct measurement of absolute emitted power.

We have measured the emissivity of high reflectivity plate samples stabilized to temperatures between 80 K and 300 K while mounted within a helium-gas cooled vacuum chamber (approximately 0.6 m in diameter and 3 m long) with base temperature near 25 K. Emitted light from the sample is detected by an ACR with an absorptivity estimated to be 99.93% in the mid-infrared, greater than 99% out to 100 µm, and greater than 97% for wavelengths out to 200 µm[4]. A cooled shutter near the sample was used to make background-subtracted measurements with the ACR. Baffles were mounted between the sample and the detector, and the vacuum chamber shrouds were coated with infrared-absorbing black paint to minimize stray light on the detector. In addition to background subtraction using the cooled shutter, two other techniques were used to minimize and quantify background effects: a set of measurements was made at very low sample temperatures (typically 20 K) in order to determine background power offsets, and temperature sensors on the shutter and chamber were used to quantify background emission levels. We have also developed and demonstrated a technique for measuring the emissivity of distinct regions of a single plate sample using the cooled shutter to partially expose the source to the detector.

## 2. Experimental methods

A schematic of the entire measurement configuration is depicted in figure 1 and a detailed view of the sample enclosure is shown in figure 2. Light is produced by the temperature-controlled sample plate, passes through the nearby source aperture and can be blocked by the cooled shutter between the source and its aperture. The emitted beam passes through a series of baffles, and light which passes through the detector aperture can be sensed by the ACR. Thermometers constantly monitor the temperatures of the sample, shutter and numerous chamber locations, such as the baffle tube nearest the sample enclosure and the chamber cold plate.

### *2.1. Detector and samples*

The National Institute of Standards and Technology (NIST) operates a number of ACRs as primary standards for optical power from visible wavelengths to the far infrared. These detectors are electrical substitution devices where a physical equivalence between incident optical power and the electrical heater power required to maintain the radiometer receiver cavity at a constant temperature can be used to define the optical power unit of the watt [8–10]. The ACR operates at liquid helium temperatures in a regime where its temperature-driven noise is minimal and where the thermal mass of its receiver is relatively small. The receiver cavity of an ACR must be designed to absorb virtually all incident optical radiation within the wavelength range of interest, so that an absolute

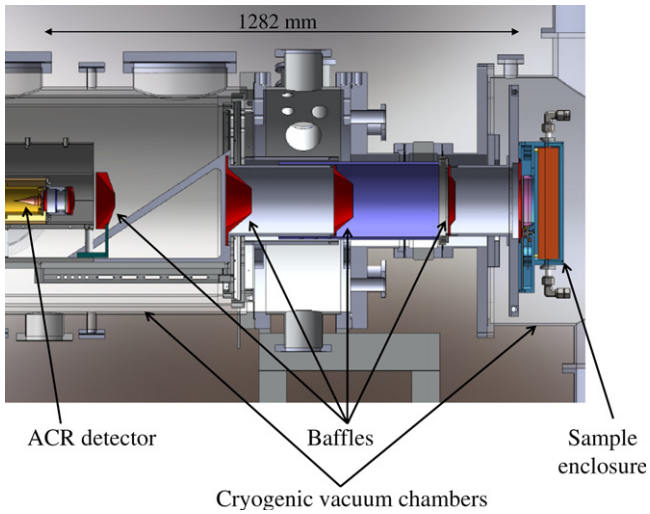


**Figure 1.** Schematic of the emissivity measurement configuration, showing the sample enclosure, ACR detector and light baffles, all contained within the cryogenic vacuum calibration chamber.

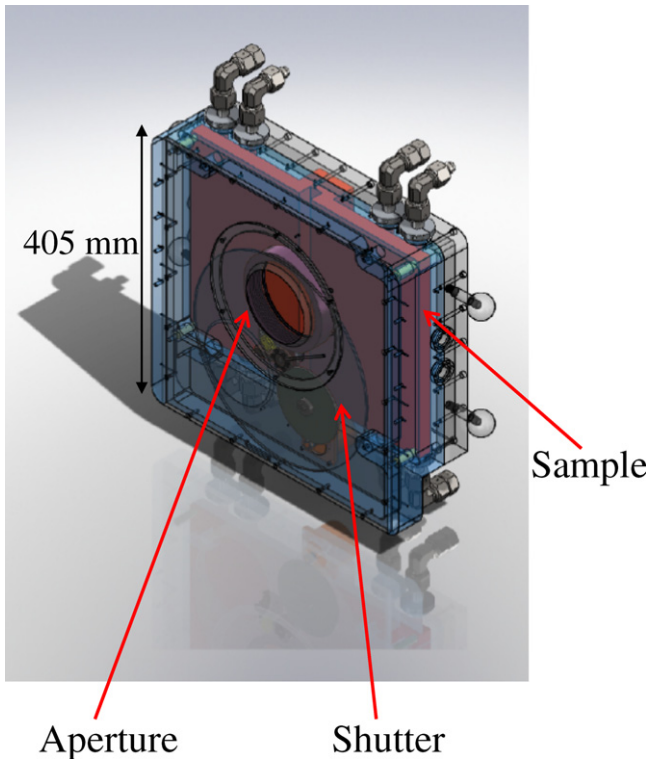


**Figure 2.** Detailed schematic of the sample enclosure, showing a mounted plate sample, the cooled shutter used for background subtraction and the sample aperture.

[4] The estimate for absorptivity is calculated from the receiver cone geometry, detector aperture size and the measured spectral absorptivity of the infrared-absorbing black paint used to coat the inside of the receiver. Data from reflectance measurements on a similar cone indicate an absorptivity of 99.94% at 10.6 µm.

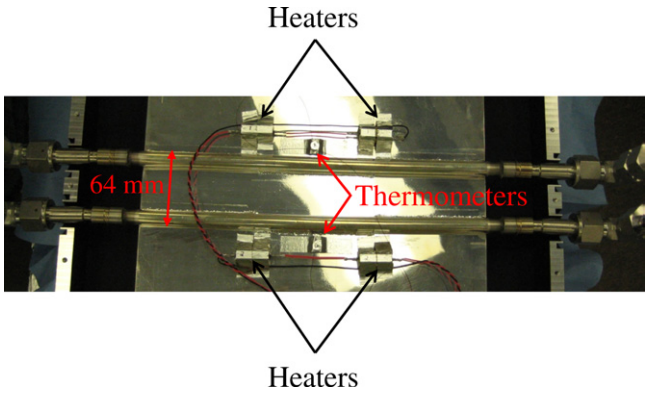


**Figure 3.** Photograph showing the temperature-control components attached to the back of a stainless steel plate sample equipped with welded cooling tubes. Two independently controllable heating zones on either side of the cooling tubes, each composed of two resistive heaters and a silicon diode thermometer, are used to maintain a constant and uniform temperature across the viewed area of the sample.

measure of the radiation entering the ACR aperture can be made. The ACR we have used has a thin-walled conical copper receiver cavity with a 30° apex angle and is coated on its inner surface with Aeroglaze Z302 infrared-absorbing black paint[5]. The noise floor is less than 10 pW for this ACR when measuring low powers and reproducibility is approximately 0.001% ($k = 1$) when measuring powers 1 μW and greater. The ACR measurement of power is background-subtracted through use of the cooled shutter near the source: first a shutter-closed measurement is made to define the background level, then the shutter is opened and the relative power change is recorded, and finally the shutter is closed again to monitor the stability of the background. The thermal response time for the ACR is approximately 17 s and a complete shutter closed–open–closed measurement generally takes about 300 s.

Our large helium-cooled vacuum chamber allows emissivity measurements of large samples, actual technical artefacts and not simply test samples, and in this paper results on stainless steel plates approximately 300 mm × 300 mm × 10 mm are presented. The plates are thermal shields made from polished 304L stainless steel and have stainless steel cooling tubes welded on one side. The plate samples are temperature-controlled using four 25 W wirewound resistive heaters arranged in a square pattern near the middle of the plate, as shown in figure 3. Two heating zones were created, each zone consisting of a pair of heaters and a nearby silicon diode thermometer, and the zones could be independently temperature-controlled to ensure uniformity of temperature across the viewed region of the source plate. Unlike most calorimetric methods, our optical method allows significant separation (greater than 1 m) between the sample and detector, so it is possible to dissipate large amounts of heat from the sample without causing significant direct or parasitic heating of the detector. This allows measurement of emissivity over a large sample temperature range from 80 K to as high as 300 K, at which temperature the total heat dissipation from the sample can be as high as 30 W. For demonstration of an emissivity determination of distinct regions on a single sample, results are also presented on a somewhat more complicated assembly consisting of two silver-coated stainless plates separated by a joint structure composed of a cavity and insulating spacer. The total size of the assembly is approximately 300 mm × 400 mm × 50 mm and the assembly is depicted in figure 4.

[5] Reference is made to commercial products to adequately specify the experimental procedures involved. Such an identification does not imply recommendation or endorsement by the National Institute of Standards and Technology, nor does it imply that these products are the best for the purpose specified.

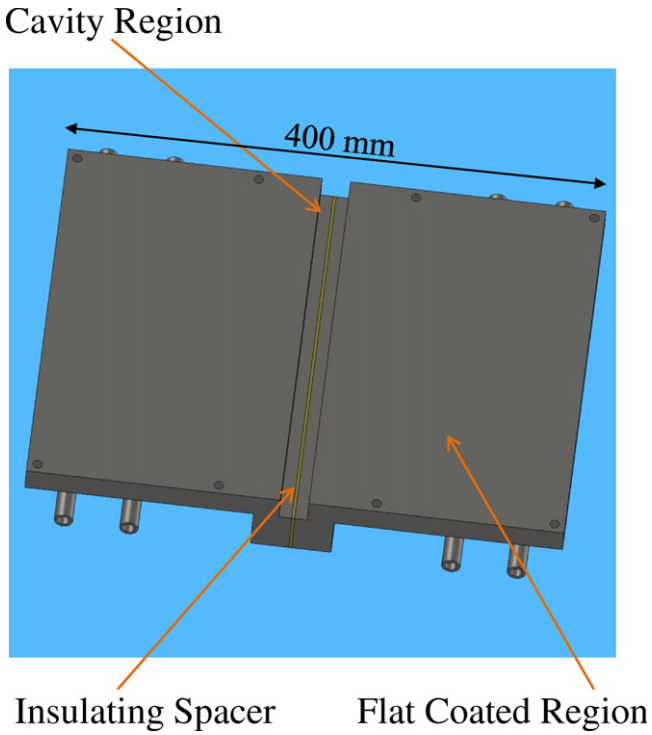


**Figure 4.** Schematic of a sample assembly used for demonstration of emissivity determination from multiple distinct regions of a single sample. The emissivities of the insulating spacer, cavity region and flat coated region were separately calculated using data from a single measurement cycle.

### 2.2. *Sample enclosure and cooled shutter*

A sample enclosure surrounds the sample plate, and this enclosure is used to mount the sample within the measurement chamber, control the thermal environment of the sample and control the light which travels from the sample to the detector. The sample enclosure is bolted to two actively cooled heat exchangers which circulate 20 K helium gas from a closed cycle helium-gas refrigerator. Mounted within the enclosure, the sample plate is isolated from the enclosure using G10 (fibreglass epoxy laminate) standoffs allowing sample temperature to be independently controlled. High-vacuum stainless steel hose is directly attached to the cooling tubes on the sample plate using high-vacuum fittings, enabling heating and cooling of the sample directly with flowing helium gas. The inside of the enclosure is coated with Aeroglaze Z306 infrared-absorbing paint (see footnote 5) to minimize light leakage, and light baffles surround the cooling tubes which penetrate the enclosure to reach the sample plate. Two critical

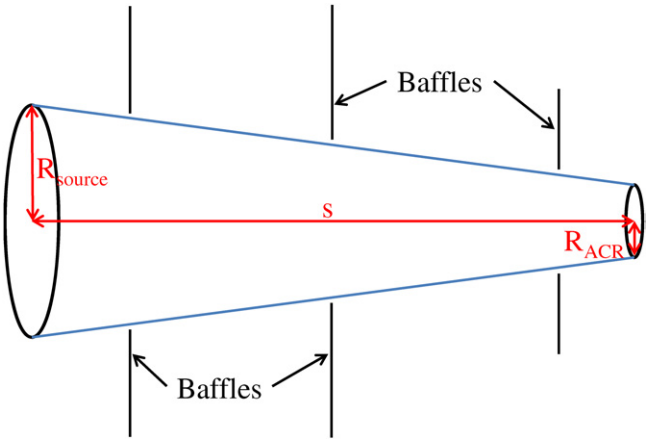


**Figure 5.** Simple diagram of the measurement geometry with dimensions critical to calculation of the configuration factor labelled. All light baffles between the source and detector apertures are non-limiting.

light-controlling features are also part of the enclosure: a rotary shutter is mounted immediately next to the sample and the 10 cm source aperture is bolted to the side of the enclosure facing the detector.

Although the rotary shutter near the source is cooled by a copper strap attached to the sample enclosure, the shutter temperature is still elevated above that of the enclosure by the radiation incident upon it from the heated sample. For accurate ACR measurements, the thermal power from the shutter itself must be estimated and includes both emitted radiation and reflection of background radiation by the shutter. The emitted shutter power is estimated using temperature data from a silicon diode thermometer on the shutter and from temperature-dependent emissivity data on the shutter material and coating. The rotary shutter used for our measurement contained an 11.4 cm diameter open position, a high-emissivity shutter position coated with Aeroglaze Z306 (see footnote 5) and a low-emissivity shutter position of polished aluminium. When reflection from background is a primary concern the Z306 position is most appropriate and when thermal emission from the shutter is of primary concern the polished aluminium position is best.

### *2.3. Distance measurement, thermometry and light baffling*

It is possible to accurately calculate the full radiant emittance (exitance) from the source aperture based on the irradiance recorded at the detector aperture because the geometry of the experiment is well-defined and precisely measured. The dimensions critical to calculation of the configuration factor for the detection throughput are the source aperture radius ($R_{\mathrm{source}}$), detector aperture radius ($R_{\mathrm{ACR}}$) and the separation distance of these two apertures ($s$) shown in figure 5. The aperture diameters were measured at room temperature using a physical contact coordinate measuring machine with an accuracy of approximately $5 \times 10^{-6}$ m, and their cryogenic dimensions were estimated using tabulated data of thermal contraction coefficients. The separation distance was determined using an *in situ* Invar measuring rod and estimates for thermal contraction of intervening metal, and this distance had a combined uncertainty ($k = 1$) of about $1.6 \times 10^{-4}$ m. Once the exitance from the source aperture is accurately determined, the emissivity of the sample can be readily calculated from the Stefan–Boltzmann law and the measured temperature of the sample plate.

Thermometry and baffling play a crucial role in quantifying and minimizing measurement uncertainties. Silicon diode thermometers on the sample, together with heaters, are used for precise temperature control of the sample plate, typically with drift of less than 10 mK in the setpoint temperature over a measurement cycle. Silicon diode thermometers on the shutter and relevant chamber components are used to quantify emittance values and uncertainties from the shutter and chamber which can affect the measured power at the ACR detector. Prior to each measurement, the system was typically allowed to stabilize for 2 h or more after the sample reached its setpoint temperature in order to minimize measured drifts. Cylindrically symmetric light baffles coated with infrared-absorbing black paint were distributed along the beam path to minimize stray light which could directly reach the detector from the chamber walls and to absorb light from the sample which could not directly reach the detector. The baffles were designed so as not to obstruct the geometric view of the source aperture from the detector aperture, as seen in figure 5, but the effect of the baffles was included in the diffraction modelling used to determine the optical throughput of the measurement system.

## 3. Analysis methods

In our measurements we employ a sensitive absolute detector in a low background environment to enable very low-temperature radiation thermometry. Particularly at the lowest sample temperatures, it is also important to quantify contributions to the power at the detector from the shutter and background in order to minimize emissivity uncertainties from particular sources to the $10^{-3}$ to $10^{-5}$ level. With reasonable temperature and emissivity uncertainties assigned to the shutter and chamber components, total emissivity uncertainties for source temperatures between 80 K and 300 K can be limited to the $10^{-3}$ to $10^{-4}$ level.

### *3.1. Light produced and light sensed*

The light produced by the sample, shutter and chamber has a thermal blackbody signature and reflection from the sample and shutter can be very significant because these elements can exhibit high reflectivity. In particular, because the sample can have emissivity much less than one (e.g. emissivity at low temperatures can be less than 0.004 for silver coatings), reflection of background signal from the sample can be a significant fraction of the sample emission, even if the background is at much lower temperature than the sample. For the sample and shutter, therefore, the emitted and reflected powers are explicitly considered as

$$S_\alpha = E_\alpha + R_\alpha = \varepsilon_\alpha \sigma T_\alpha^4 + (1 - \varepsilon_\alpha)\sigma \varepsilon_{\mathrm{b}} T_{\mathrm{b}}^4, \qquad \alpha \in \{\mathrm{s}, \mathrm{sh}\} \tag{1}$$

where $S_\alpha$ is the total power from a particular source, $E_\alpha$ is the emitted part and $R_\alpha$ is the reflected part. The emissivity of a particular source is $\varepsilon_\alpha$ and its temperature is $T_\alpha$. The source subscripts s, sh and b refer to the sample, shutter and background, respectively, and $\sigma$ is the Stefan–Boltzmann constant. Most light which reaches the detector directly from the chamber background is subtracted off by the shutter-closed, shutter-open difference measurement made by the ACR. To first order, the scene from the background presented to the detector with shutter closed or shutter open is identical, so when the difference of the shutter-closed and shutter-open measurements is taken, the direct background effect is mostly nullified. There may be a small offset between the direct background contribution in the shutter-closed and shutter-open measurements, however, caused by leakage from the sample enclosure in the shutter-open position or by a difference-in-scene dependent on shutter position. This additional offset can be subtracted off by making measurements at very low sample temperatures as will be described below.

Light reaching the detector from the sample and shutter is defined by geometry and modulated by diffraction effects. For two circular apertures with a common normal axis the configuration factor $F$ is given by

$$F = \frac{1}{2}[z - [z^2 - 4x^2y^2]^{1/2}], \tag{2}$$

where

$$x = \frac{r_2}{s}, \qquad y = \frac{s}{r_1}, \qquad z = 1 + [1 + x^2]y^2$$

and $r_1$ is the radius of the source aperture, $r_2$ is the radius of the detector aperture and $s$ is the separation distance between the apertures. If a power-scaled configuration factor is defined by $\Gamma = \sigma A F$, where $\sigma$ is the Stefan–Boltzmann constant and $A$ is the area of the source aperture, then the power measured by the ACR directly from the sample emittance can be simply written as $E_\mathrm{s} = \varepsilon_\mathrm{s}\Gamma T_\mathrm{s}^4$. Of course, emission from the shutter and reflected terms must also be considered. For instance, the reflected term from the sample is $R_\mathrm{s} = (1 - \varepsilon_\mathrm{s})\varepsilon_\mathrm{b}\Gamma T_\mathrm{b}^4$. It must also be noted that the emissivities of the sample, shutter and background are dependent upon wavelength and source temperature.

Diffraction corrections for our particular measurement geometry have been calculated using a method based on Kirchhoff diffraction theory generally applicable to cylindrically symmetric systems [11, 12]. Taking into account diffraction from limiting and non-limiting apertures and baffles, modifications to the geometric throughput can be calculated and results can be compactly reported as the 'diffraction factor' $\mathscr{D} = P/P_0$, where $P$ is the expected power at the detector including diffraction effects and $P_0$ is the expected power at the detector considering only geometrical optics. Computer code written at NIST has been used to calculate diffraction factors for our measurement geometry over a wavelength range from 2 µm to 4 mm. Diffraction effects for light produced by the sample, shutter and chamber were properly weighted depending on the temperature of the source.

The power recorded at the ACR detector during a single measurement at a particular sample setpoint temperature is a difference of shutter-open and shutter-closed powers. This net power is equal to a combination of emitted and reflected light from sample and shutter and must take into account wavelength-dependent diffraction effects. The power measured at a sample setpoint temperature $T_\mathrm{s} = T_\mathrm{set}$ is given by

$$(S_\mathrm{s} - S_\mathrm{sh})^{(\mathrm{meas})}_{|T_\mathrm{s}=T_\mathrm{set}} = [\varepsilon_\mathrm{s}\Gamma T_\mathrm{s}^4\mathscr{D}_\mathrm{s} - \varepsilon_\mathrm{s}\Gamma\varepsilon_\mathrm{b}T_\mathrm{b}^4\mathscr{D}_\mathrm{b} - \varepsilon_\mathrm{sh}\Gamma T_\mathrm{sh}^4\mathscr{D}_\mathrm{sh} + \varepsilon_\mathrm{sh}\Gamma\varepsilon_\mathrm{b}T_\mathrm{b}^4\mathscr{D}_\mathrm{b}]_{|T_\mathrm{s}=T_\mathrm{set}} \tag{3}$$

where $\mathscr{D}_\mathrm{s}$, $\mathscr{D}_\mathrm{sh}$ and $\mathscr{D}_\mathrm{b}$ are the diffraction factors for light from the sample, shutter and background, respectively. Each of the sources has emissivity $\varepsilon_\alpha$ and temperature $T_\alpha$, where $\alpha \in \{\mathrm{s}, \mathrm{sh}, \mathrm{b}\}$. Given the low background temperature and the shutter method of background subtraction, terms related to direct illumination of the detector by the background should be very small. There is, however, the possibility for a small power offset related to leakage radiation from the sample enclosure or to differences in background-scene dependent on the shutter position. This offset can be accounted for by making measurements with the sample plate at a very low base temperature, typically 20 K. Since the sample has low emissivity and is very cold, the signals from the shutter and any possible offset dominate such an ACR measurement and the sample contribution is negligible. Assuming that the offset is approximately constant, at least for low sample temperatures, it is possible to subtract off the offset from the emissivity determination by considering the difference between the emittance at the setpoint temperature and the emittance at the base temperature. Any differential leakage originating from the heated sample is not included in this measured offset, and it is assumed that such leakage (which must be different in the shutter-open and shutter-closed positions to contribute) is negligible.

### 3.2. Calculation of emissivity and its related uncertainty

Using equation (3) and subtracting off the potential power offset with the base temperature ACR measurement, one can express the sample emissivity as

$$\begin{aligned}\varepsilon_{\mathrm{s}|T_\mathrm{s}=T_\mathrm{set}} = {} & \left(\frac{(S_\mathrm{s} - S_\mathrm{sh})^{(\mathrm{meas})}}{\mathscr{D}_\mathrm{s}}_{|T_\mathrm{s}=T_\mathrm{set}} - \frac{(S_\mathrm{s} - S_\mathrm{sh})^{(\mathrm{meas})}}{\mathscr{D}_\mathrm{sh}}_{|T_\mathrm{s}=T_\mathrm{base}}\right) \Bigg/ (\Gamma T_\mathrm{s}^4)_{|T_\mathrm{s}=T_\mathrm{set}} \\ & + \left(\left[\varepsilon_\mathrm{sh}T_\mathrm{sh}^4\frac{\mathscr{D}_\mathrm{sh}}{\mathscr{D}_\mathrm{s}} - (\varepsilon_\mathrm{sh} - \varepsilon_\mathrm{s}^{(0)})\varepsilon_\mathrm{b}T_\mathrm{b}^4\frac{\mathscr{D}_\mathrm{b}}{\mathscr{D}_\mathrm{s}}\right]_{|T_\mathrm{s}=T_\mathrm{set}}\right. \\ & \left. + \left[\varepsilon_\mathrm{s}^{(0)}T_\mathrm{s}^4\frac{\mathscr{D}_\mathrm{s}}{\mathscr{D}_\mathrm{sh}} - \varepsilon_\mathrm{sh}T_\mathrm{sh}^4 + (\varepsilon_\mathrm{sh} - \varepsilon_\mathrm{s}^{(0)})\varepsilon_\mathrm{b}T_\mathrm{b}^4\frac{\mathscr{D}_\mathrm{b}}{\mathscr{D}_\mathrm{sh}}\right]_{|T_\mathrm{s}=T_\mathrm{base}}\right) \Bigg/ (T_\mathrm{s}^4)_{|T_\mathrm{s}=T_\mathrm{set}},\end{aligned} \tag{4}$$

where the first two terms on the right-hand side are from the ACR measurements and the other terms are composed of measured temperatures and measured or tabulated emissivities. The notation '$|T_\mathrm{s} = T_\mathrm{set}$' or '$|T_\mathrm{s} = T_\mathrm{base}$' indicates that the relevant terms are measured or calculated for the sample at a setpoint temperature $T_\mathrm{set}$ (various temperatures between

80 K and 300 K) or at the sample base temperature $T_{\text{base}}$ (typically 20 K). The $\varepsilon_{\text{s}}^{(0)}$ term is a first order estimate of sample emissivity given by just the first two terms on the right-hand side of equation (4), neglecting the shutter and background correction terms. The additional background, shutter and diffraction terms apart from the ACR measurement values are small, typically around 2% of the total emissivity at 80 K and 0.2% of the emissivity at 300 K.

The calculation of uncertainty in the sample emissivity is straightforward if somewhat tedious. First the uncertainty of each of 21 distinct measured or tabulated parameters on the right-hand side of equation (4) was calculated or estimated. For the ACR data and some of the dimension data, type A uncertainties were calculated from multiple measurements. Type B estimates were used for uncertainties in emissivities, temperatures and diffraction factors. The uncertainty of the power-scaled configuration factor $\Gamma$ was determined by propagating the uncertainties of the aperture radii and their separation distance using the relations of equation (2). With uncertainties assigned to $\Gamma$ and to the 10 distinct parameters at each of the two temperatures $T_{\text{set}}$ and $T_{\text{base}}$, the uncertainties were propagated based on equation (4) to determine the uncertainty in sample emissivity at a temperature $T_{\text{set}}$. Most parameters were assumed independent but possible correlations between temperature readings and emissivity values at $T_{\text{set}}$ and $T_{\text{base}}$ were taken into consideration.

### *3.3. Emissivity of multiple distinct regions on a single sample*

The use of an optical measurement technique of emissivity, where the source and detector are well separated, makes it practical to use a shutter to quantify the emissivity from different distinct regions of a sample plate. In the case illustrated here using the sample depicted in figure 4, we used the shutter to expose three different regions at each setpoint temperature where emissivity was determined. In the first shutter position (fully open), all three sample regions were exposed to the detector, in the second shutter position only the cavity region and flat part of the plate were exposed, and in the final shutter position only the flat part of the plate was exposed. For each shutter position, the configuration factor for the exposed area could be numerically computed from the general configuration factor expression:

$$F = \frac{1}{A_1 \pi} \int_{A_1} \int_{A_2} \frac{\mathrm{d}A_1 \cos\theta_1 \, \mathrm{d}A_2 \cos\theta_2}{R^2}, \tag{5}$$

where $A_1$ is the area of the exposed section of the sample, $A_2$ is the area of the sample aperture, $R$ is the distance between the area elements of integration $\mathrm{d}A_1$ and $\mathrm{d}A_2$, and $\theta_1$ and $\theta_2$ are the angles between the normals to the area elements and the line connecting the area elements [13]. Using these computed configuration factors and the analysis methods for emissivity described, the effective emissivity of each exposed area was calculated at each setpoint temperature.

At least in the far-field approximation, the emissivity of each distinct sample region can be determined from the emissivity of the three exposed areas and the relative contribution to the configuration factor from each sample region. Let $F_j^{(k)}$ be the configuration factor for the $j$th region of the sample, $j \in \{1, 2, 3\}$, in the case where the shutter exposed $k$ of the three sample regions, $k \in \{\text{i}, \text{ii}, \text{iii}\}$. Then define $\mathscr{F}_j^{(k)} = F_j^{(k)} / \sum_{j=1}^{3} F_j^{(k)}$ as the fractional configuration factor of region $j$ and note that $\sum_{j=1}^{3} \mathscr{F}_j^{(k)} = 1$. The emissivity measured is then constituted from the emissivities of each sample region in the following way:

$$\begin{aligned} \varepsilon_{\text{i}}^{(\text{meas})} &= \varepsilon_1 \\ \varepsilon_{\text{ii}}^{(\text{meas})} &= \mathscr{F}_2^{(\text{ii})} \varepsilon_2 + \mathscr{F}_1^{(\text{ii})} \varepsilon_1 \\ \varepsilon_{\text{iii}}^{(\text{meas})} &= \mathscr{F}_3^{(\text{iii})} \varepsilon_3 + \mathscr{F}_2^{(\text{iii})} \varepsilon_2 + \mathscr{F}_1^{(\text{iii})} \varepsilon_1. \end{aligned} \tag{6}$$

And the emissivities of the distinct plate regions can be determined from the measured emissivity according to the following equations:

$$\begin{aligned} \varepsilon_1 &= \varepsilon_{\text{i}}^{(\text{meas})} \\ \varepsilon_2 &= (\varepsilon_{\text{ii}}^{(\text{meas})} - \mathscr{F}_1^{(\text{ii})} \varepsilon_1) / \mathscr{F}_2^{(\text{ii})} \\ \varepsilon_3 &= (\varepsilon_{\text{iii}}^{(\text{meas})} - \mathscr{F}_2^{(\text{iii})} \varepsilon_2 - \mathscr{F}_1^{(\text{iii})} \varepsilon_1) / \mathscr{F}_3^{(\text{iii})}. \end{aligned} \tag{7}$$

The uncertainty for the fractional configuration factors can be determined from the uncertainties of measured dimensional values as well as uncertainty in the shutter position. The uncertainties for the calculated emissivities for each sample region can be determined from propagation of uncertainties with equations (7), using the calculated uncertainties in the measured emissivities and fractional configuration factors.

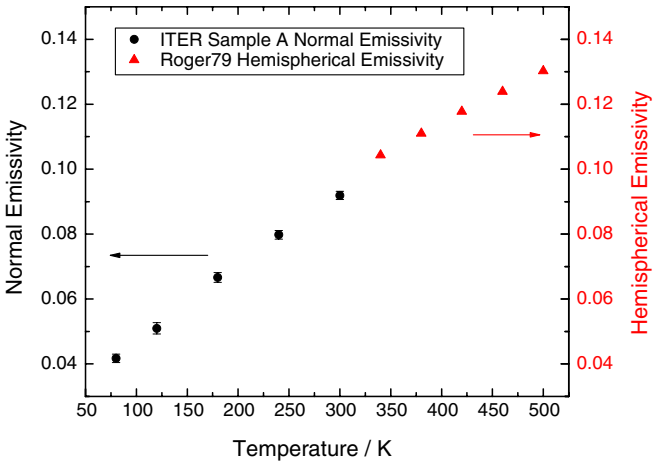


**Figure 6.** Normal emissivity as a function of temperature for a polished 304L stainless steel plate sample measured at temperatures from 80 K to 300 K. Hemispherical emissivity data from the literature [7] for temperatures of 340 K and greater are plotted together with our data for comparison. Error bars denote the standard deviations of our measured emissivities.

## 4. Example measurement results

Emissivity results at temperatures between 80 K and 300 K are shown in figure 6 for the polished 304L stainless steel plate with welded cooling tubes described in section 2. The error bars show the standard deviations at each temperature setpoint,

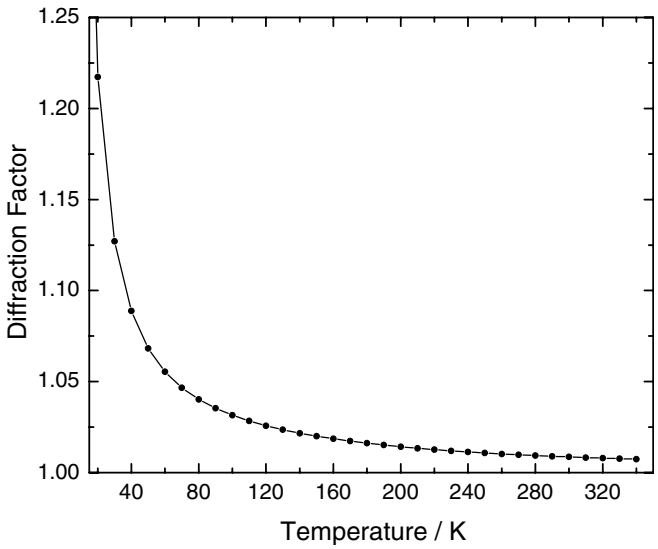


**Figure 7.** Calculated diffraction factor for our measurement geometry as a function of temperature. At 80 K the adjustment of throughput from diffraction is approximately 4% and at 300 K it is approximately 0.86%.

and data from the literature at higher temperatures for polished 304 stainless steel are plotted in the same figure. The data from Roger *et al* [7], determined using a dynamic calorimetry method, span the range from 340 K to 1100 K and provide the hemispherical emissivity rather than the normal emissivity as is determined by our method. There is no simple relationship between hemispherical emissivity and normal emissivity for a 'poor' conductor such as stainless steel, but Sievers has calculated that the two emissivities are nearly equal for metals which exhibit dc resistivities similar to stainless steel [14]. There is good agreement between the temperature-dependent slope in emissivity for our data and that of Roger *et al*. For our measurements, it should be noted that the inclusion of diffraction effects in the analysis was important because these effects can make a significant difference in recorded power. The adjustment of throughput from diffraction for our optical arrangement is approximately 4% at 80 K and falls to 0.86% at 300 K as shown in figure 7.

The contributions from all experimental parameters in equation (4) to the uncertainty of the calculated emissivity of the polished 304L stainless steel plate at a setpoint temperature of 80 K are presented in table 1. Each entry in the list, other than the power-scaled configuration factor $\Gamma$, includes uncertainty contributions for each parameter at both the setpoint temperature $T_{\mathrm{set}}$ and the base temperature $T_{\mathrm{base}}$ because emissivity is calculated from a difference of the data at the setpoint and base temperatures. Uncertainty scales roughly with emissivity so for other samples where the emissivity was less than 0.01, we have found that the total uncertainty in the calculated emissivity can be as low as 0.000 13.

The method described in section 3 to extract emissivities of multiple distinct regions of a single sample was used for the sample shown in figure 4 and described in section 2. That the ACR detector can easily detect the emissivity differences between exposed sample regions as the sample shutter is rotated can be seen in figure 8. In the figure, optical power

**Table 1.** Example of the uncertainty contributions to the calculated emissivity from various experimental parameters for the polished stainless steel plate sample at setpoint temperature 80 K. For each parameter in the list other than the power-scaled configuration factor $\Gamma$, the uncertainty represents a combination of the uncertainty at the setpoint temperature ($T_{\mathrm{set}} = 80$ K) and the base temperature ($T_{\mathrm{base}} = 20$ K).

| Experimental parameter | Contribution to emissivity uncertainty |
|---|---|
| $(S_{\mathrm{s}} - S_{\mathrm{sh}})^{(\mathrm{meas})}$ | $1.160 \times 10^{-4}$ |
| $T_{\mathrm{s}}$ | $4.173 \times 10^{-4}$ |
| $T_{\mathrm{sh}}$ | $1.673 \times 10^{-5}$ |
| $T_{\mathrm{b}}$ | $4.217 \times 10^{-4}$ |
| $\varepsilon_{\mathrm{sh}}$ | $1.015 \times 10^{-4}$ |
| $\varepsilon_{\mathrm{b}}$ | $4.390 \times 10^{-5}$ |
| $\varepsilon_{\mathrm{s}}^{(0)}$ | $9.362 \times 10^{-4}$ |
| $\mathscr{D}_{\mathrm{s}}$ | $7.360 \times 10^{-5}$ |
| $\mathscr{D}_{\mathrm{sh}}$ | $2.183 \times 10^{-5}$ |
| $\mathscr{D}_{\mathrm{b}}$ | $4.931 \times 10^{-6}$ |
| $\Gamma$ | $1.111 \times 10^{-4}$ |
| Total | $1.128 \times 10^{-3}$ |

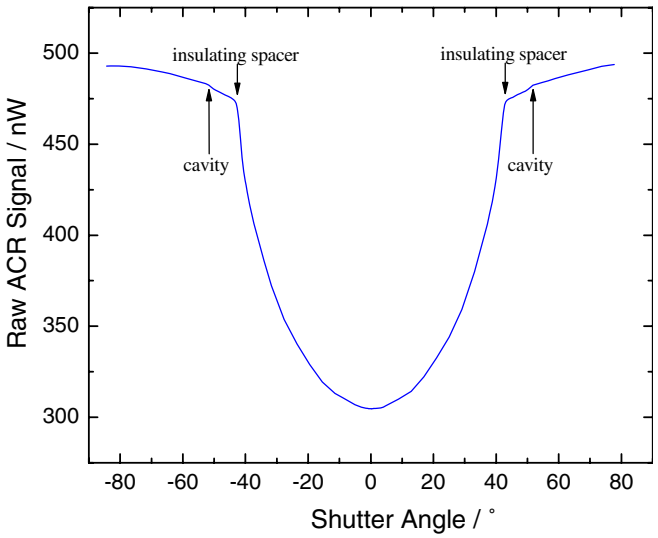


**Figure 8.** Detector signal plotted as a function of shutter angle for the measurement of the sample assembly illustrated in figure 4. Clear features are evident in the data as the shutter exposes new distinct regions of the sample to the detector. The raw detector signal decreases when the light reaching it increases.

measured at the detector is plotted as a function of shutter rotation relative to a fully open position. Clear junctions of slope change occur as the shutter exposes new distinct regions of the sample which were previously blocked from the detector. The standard deviations for the emissivities of the different sample regions at a temperature of 80 K ranged from 0.0004 for the flat region (large area, low emissivity) to 0.054 for the insulating spacer (small area, high emissivity).

## 5. Summary and conclusions

An optical method for determining the low-temperature absolute emissivity of samples with high accuracy has been developed. The technique has been demonstrated on

low emissivity, large area artefacts at setpoint temperatures between 80 K and 300 K. Absolute errors and background effects are reduced by the use of a high sensitivity primary standard detector operated in a background-subtracted mode employing a cooled shutter. Offset subtraction at low sample temperature and background power quantification based on shutter and chamber thermometry help one to further reduce uncertainties in the technique. Our method enables low-temperature emissivity calibration of technologically important components, so that estimates for their cryogenic emissivity need not be extrapolated from higher temperature values. In the emissivity measurement technique described the detector is greater than 1 m from the sample so it could be possible to mount the sample on a rotating platform and acquire cryogenic effective emissivity data on a complicated sample as viewed from numerous angles.

## References


[1] Ageladarakis P A and Obert W 1998 On the emissivity of silver coated panels, effect of long term stability and effect of coating thickness *Cryogenic Engineering Conf. 1998 (Bournemouth, UK)* ed D DewHughes *et al* pp 715–8

[2] Lipa M, Martinez A, Lacroix B and Chatain D 2009 Experience with silver coated vacuum vessel thermal shield at 80 K in Tore Supra *23rd IEEE/NPSS Symp. on Fusion Engineering (San Diego, CA)* pp 603–6

[3] Herve P, Rambure N, Sadou A, Ramel D, Francou L, Delouard P and Gavila E 2008 Direct measurement of total emissivities at cryogenic temperatures: application to satellite coatings *Cryogenics* **48** 463–8

[4] Tolson W, Or C, Glazer S, Kobel M and Packard E 2005 Determination of coating emittance at cryogenic temperatures for the James Webb Space Telescope—experimental methods and results *Cryogenic Optical Systems and Instruments XI* ed J B Heaney and L G Burriesci *Proc. SPIE* **5904** 59040G

[5] Or C, Tolson W, Glazer S, Kobel M and Packard E 2005 Cryogenic emittance measurement and its accuracy for the James Webb Space Telescope *Cryogenic Optical Systems and Instruments XI* ed J B Heaney and L G Burriesci *Proc. SPIE* **5904** 59040H

[6] Musilova V, Hanzelka P, Kralik T and Srnka A 2005 Low temperature radiative properties of materials used in cryogenics *Cryogenics* **45** 529–36

[7] Roger C R, Yen S H and Ramanathan K G 1979 Temperature variation of total hemispherical emissivity of stainless steel AISI 304 *J. Opt. Soc. Am.* **69** 1384–90

[8] Datla R U, Stock K, Parr A C, Hoyt C C, Miller P J and Foukal P V 1992 Characterization of an absolute cryogenic radiometer as a standard detector for radiant-power measurements *Appl. Opt.* **31** 7219–25

[9] Houston J M and Rice J P 2006 NIST reference cryogenic radiometer designed for versatile performance *Metrologia* **43** S31–5

[10] Carter A C, Lorentz S R, Jung T M and Datla R U 2005 ACRII: Improved absolute cryogenic radiometer for low background infrared calibrations *Appl. Opt.* **44** 871–5

[11] Shirley E L and Terraciano M L 2001 Two innovations in diffraction calculations for cylindrically symmetric systems *Appl. Opt.* **40** 4463–72

[12] Shirley E L 2005 Diffraction effects in radiometry *Optical Radiometry* ed A C Parr *et al* (San Diego, CA: Elsevier Academic Press) pp 409–51

[13] Datla R U and Parr A C 2005 Introduction to optical radiometry *Optical Radiometry* ed A C Parr *et al* (San Diego, CA: Elsevier Academic Press) pp 1–34

[14] Sievers A J 1978 Thermal radiation from metal surfaces *J. Opt. Soc. Am.* **68** 1505–16